ACS SENSORS

pubs.acs.org/acssensors
Letter

Improvement of the Green−Red Förster Resonance Energy Transfer-Based Ca^{2+} Indicator by Using the Green Fluorescent Protein, Gamillus, with a Trans Chromophore as the Donor

Tomoki Matsuda,* Shinya Sakai, Kei-ichi Okazaki, and Takeharu Nagai*

Cite This: *ACS Sens.* 2024, 9, 1743−1748

ABSTRACT: To monitor the Ca^{2+} dynamics in cells, various genetically encoded Ca^{2+} indicators (GECIs) based on Förster resonance energy transfer (FRET) between fluorescent proteins are widely used for live imaging. Conventionally, cyan and yellow fluorescent proteins have been often used as FRET pairs. Meanwhile, bathochromically shifted indicators with green and red fluorescent protein pairs have various advantages, such as low toxicity and autofluorescence in cells. However, it remains difficult to develop them with a similar level of dynamic range as cyan and yellow fluorescent protein pairs. To improve this, we used Gamillus, which has a unique trans-configuration chromophore, as a green fluorescent protein. Based on one of the best high-dynamic-range GECIs, Twitch−NR, we developed a GECI with 1.5-times higher dynamic range (253%), Twitch−GmRR, using RRvT as a red fluorescent protein. Twitch−GmRR had high brightness and photostability and was successfully applied for imaging the Ca^{2+} dynamics in live cells. Our results suggest that Gamillus with trans-type chromophores contributes to improving the dynamic range of GECIs. Therefore, selection of the cis−trans isomer of the chromophore may be a fundamental approach to improve the dynamic range of green−red FRET indicators, unlimited by GECIs.

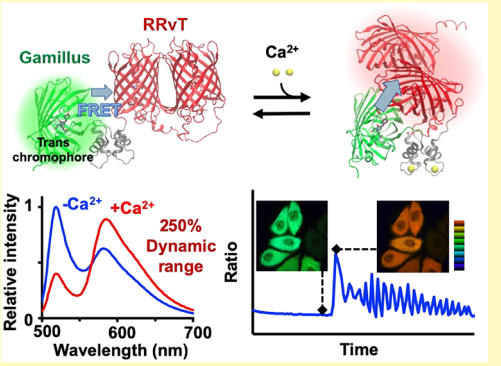

KEYWORDS: *fluorescent protein, Förster resonance energy transfer, fluorescent indicator, genetically encoded Ca^{2+} indicators, protein engineering*

To determine the role of Ca^{2+} signaling at different spatiotemporal scales, Ca^{2+} imaging technology has been extensively developed and several Ca^{2+} indicators are currently available for living cells. For example, fluorescent protein (FP)-based genetically encoded Ca^{2+} indicators (GECIs) using Förster resonance energy transfer (FRET) consist of a Ca^{2+} sensing domain and a FRET FP pair fused to its termini. Ca^{2+}-dependent structural changes in the Ca^{2+}-sensing domain cause a shift in the relative distance and orientation of the terminal FRET FP pair, resulting in reciprocal fluorescence intensity changes owing to the changes in the FRET efficiency. Compared to single FP-based indicators, FRET-based indicators, which require two optical channels, are disadvantagious for multicolor imaging.[1] FRET-based indicators are also inferior to single FP-based indicators with smaller intensity changes and slower kinetics. However, they can perform imaging free from any intensity fluctuations owing to changes in the indicator concentration and focal position by generating an intensity ratio image between the FRET acceptor and donor channels. Although intensity-independent imaging with single FP-based indicators is possible using fluorescence lifetime imaging microscopy (FLIM) or excitation-ratiometric indicators, these require complicated and expensive optical setups or currently have a limited number of indicators available. FRET-based indicators also do not show significantly low intensity at low Ca^{2+} levels that generally occur with most intesiometric single FP-based indicators, thus enabling the imaging of the distribution pattern of indicators localized in the subcellular space with a high signal-to-noise ratio. Many of these drawbacks and advantages relate to the usability of currently available indicators rather than their fundamental nature, but they are important points for the development of practically useful indicators.

Cyan FPs (CFPs) and yellow FPs (YFPs) are the most widely used pairs for the development of FRET-based indicators. To date, they and their circular permutants are used in FRET-based indicators with high dynamic range, such as the Cameleon and Twitch series with calmodulin-M13 and troponin C (TnC) derivative as the Ca^{2+} sensing domains, respectively.[2−4] However, the violet excitation light of CFP for

Received: November 11, 2023
Revised: February 29, 2024
Accepted: March 6, 2024
Published: March 22, 2024

https://doi.org/10.1021/acssensors.3c02398
ACS Sens. 2024, 9, 1743−1748

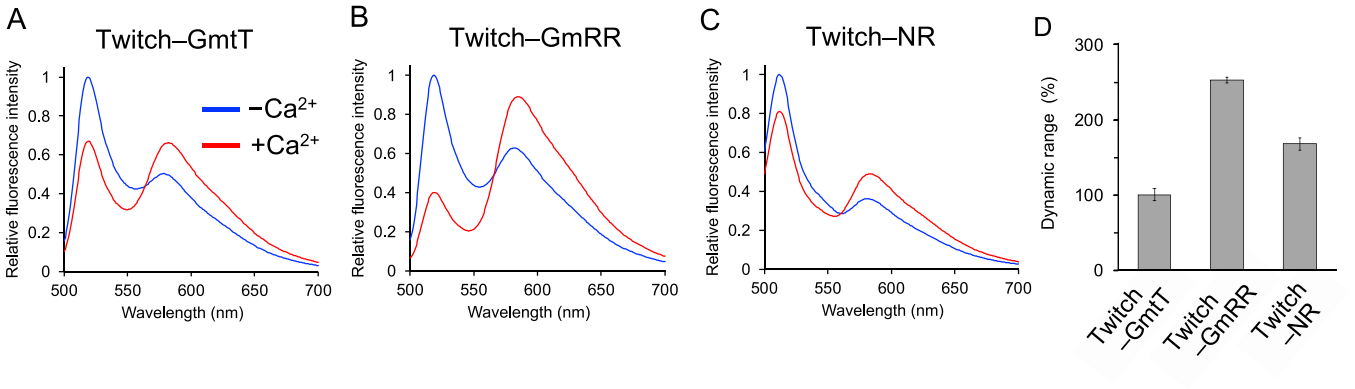

Figure 1. Ca^{2+} response of Twitch−GmRR and the other variants. Fluorescence spectra in the absence (10 mM EGTA) and saturated Ca^{2+} (1 mM $CaCl_2$) conditions are indicated by blue and red lines, respectively, for Twitch−GmtT (A), Twitch−GmRR (B), and Twitch−NR (C). (D) Dynamic range of the green−red Twitch variants. Dynamic range was calculated using the following formula: $\frac{R_{+Ca} - R_{-Ca}}{R_{-Ca}}$, where R_{-Ca} and R_{+Ca} indicate the fluorescence intensities ratio in the absence of Ca^{2+} and with saturated Ca^{2+}, respectively (n = 4, error bar represents ± SD).

FRET imaging can lead to problems, such as cell phototoxicity, autofluorescence of cell components, and scattering in tissues.[5−7] To address this situation, bathochromically shifted FRET indicators with green FP (GFP) and red FP (RFP) pairs have been developed for several types of indicators, including GECIs.[8−12] Although they induce a change in acceptor/donor intensity ratio in response to the change in concentration of their targets, their dynamic range is significantly smaller than that of the CFP−YFP FRET-based GECIs with an over 500% dynamic range. To improve this situation, we aimed to use a new GFP, Gamillus.[13] Gamillus has a chromophore in the trans configuration that is isomeric to the chromophores of general GFPs in the cis configuration. In some cases, mRuby2 or mRuby3 with chromophores in the trans configuration have been used as GFP−RFP FRET-based indicators.[8−10] However, donor FP with chromophores in the trans configuration has not yet been used for the development of GFP−RFP FRET-based indicators. Expecting the chromophore of the donor with a trans configuration and high quantum yield (0.9) to change this situation, we developed a GFP−RFP FRET-based GECI using Gamillus without circular permutation as a donor in this study.

RESULTS AND DISCUSSION

Optimization of the Linker Sequence of the Gamillus−tdTomato FRET GECI. Following the recently developed high-dynamic-range GECIs with circularly permuted green and normal red FP pairs, Twitch−NR,[11] we used a Ca^{2+}-sensing domain derived from TnC. Gamillus and tdTomato, which showed high FRET efficiency in the tandem fusion construct with Gamillus (Text S1; Table S1; Figure S1), were fused to the N- and C-termini of TnC, respectively. In the design of FRET-based GECIs, linker sequences influence their performance. In the case of Twitch−2B, which is the ancestral cyan−yellow FRET GECI of Twitch−NR, the linker sequences were optimized by screening, and their helical motifs were well-integrated into the Ca^{2+}-bound TnC in the crystal structure to be compact, resulting in high FRET efficiency.[4,14] To investigate the effect of these linkers (VADA and PIYP linkers located at the N- and C-termini of TnC, respectively) on the Gamillus−tdTomato FRET GECI, we tested constructs with and without them *in vitro*. In addition to the full-length FPs, we also used FPs with deletion of the flexible end (Gamillus with C-terminal 9 amino acid deletion (GamillusΔC9) and tdTomato with N-terminal 11 amino acid deletion (tdTomatoΔN11)) to reduce the influence of the flexible terminal regions on the spacing of the FPs. Comparing the cases with and without linkers, the latter tended to have a higher dynamic range of intensity ratios between the $-Ca^{2+}$ and saturated Ca^{2+} conditions (Figure S2). For constructs without linkers, the dynamic range was higher in the case of terminally deleted FPs. As a further attempt, we measured the case with only the C-terminal PIYP linker, which is expected from the determined structure to contribute to the reduction of the dynamics in the Ca^{2+}-bound state.[14] Fortunately, this construct GamillusΔC9−TnC−PIYP−tdTomatoΔN11 (Twitch−GmtT) had a higher dynamic range than the others (Figure S2). It is not easy to find a strict interpretation, but the intensity ratio in the $-Ca^{2+}$ and saturated Ca^{2+} conditions suggests that the lower intensity ratio in the $-Ca^{2+}$ condition contributed to a higher dynamic range (Figure S3).

Substitution of tdTomato with the High Quantum Yield Variant, RRvT. There is a variant of tdTomato called RRvT, which has a slightly lower molar extinction coefficient (tdTomato 138 × 10^3; RRvT 134 × 10^3 M^{-1} cm^{-1}), but a higher quantum yield (tdTomato 0.69; RRvT 0.88).[15] Although theoretically the FRET efficiency is not affected by the quantum yield of the acceptor FP, a higher quantum yield resulting in higher sensitized emission has the potential to improve the dynamic range for the ratio imaging.[16−18] To test this possibility, we generated Twitch−GmRR by substituting the tdTomato moiety in Twitch−GmtT with N-terminally deleted RRvT (Table S2). This substitution had a beneficial effect and Twitch−GmRR showed a higher dynamic range (253%) than the ancestral Gamilus-tdTomato FRET GECIs (less than 101%) (Figure 1A, B, and D; Figure S2). Twitch−GmRR showed a much larger decrease in the donor fluorescence from $-Ca^{2+}$ to saturated Ca^{2+} conditions (approximately 2-fold) than Twitch−GmtT, suggesting a large change in FRET efficiency. This implies that the improvement in Twitch−GmRR is due to a large contribution from the effect of the configuration change, including the relative orientation of the chromophores. We also directly compared the dynamic range with that of Twitch−NR, which has been reported to show large changes in FRET efficiency between the Ca^{2+}-resting and Ca^{2+}-saturated states.[11] Com-

https://doi.org/10.1021/acssensors.3c02398
ACS Sens. 2024, 9, 1743−1748

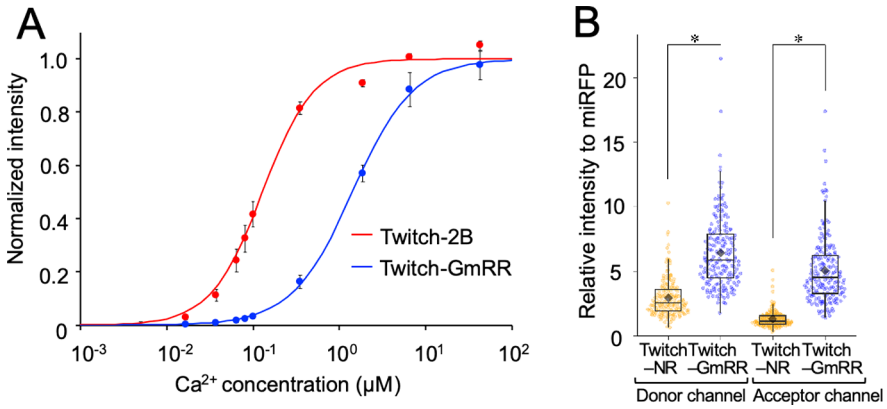

Figure 2. Characteristics of Twitch−GmRR. (A) Ca^{2+} titration curve measured *in vitro* (n = 3, Error bar represents ± SD). (B) Dot plot overlaid on a box plot of the relative fluorescent intensity of Twitch−NR and Twitch−GmRR to the reference miRFP for donor and acceptor channels in HeLa cells. Black diamonds indicate the mean values (*p < 0.05, two-sided Wilcoxon rank-sum test; $n \geq 173$ cells for each). Results for 190 cells from 34 dish cultures and 174 cells from 34 dish cultures are shown for Twitch−NR and Twitch−GmRR, respectively.

pared to Twitch−NR with 168% dynamic range, Twitch−GmRR had 1.5-times higher dynamic range of 253% (Figure 1C and D), indicating the desirable effects of the trans chromophore of Gamillus. Variants of Twitch−GmRR in which the Gamillus moiety was replaced by other GFPs, mNeonGreen, or EGFP had less than half the dynamic range of Twitch−GmRR (Figure S4). This supports the idea that the improvement is due to the effect of the trans chromophore GFP rather than the contribution of the generally better property of the FRET acceptor RRvT in any GFP.

Characterization of Twitch−GmRR. To assess the applicability of Twitch−GmRR for live-cell imaging, we characterized its properties. We analyzed its affinity for Ca^{2+} in solution via Ca^{2+} titration, and the determined K_d value (1.41 μM) was larger than that of Twitch−2B (128 nM in this work and 200 nM in the reference paper, respectively) and Twitch−NR (610 nM in the reference paper) (Figure 2A; Table 1). This K_d value was comparable to the K_d values of

Table 1. Ca^{2+} Affinities of Different Twitch Variants

	K_d (nM)	ref
Twitch−2B	128	this work
	200	11
Twitch−NR	610	11
Twitch−GmRR	1410	this work

Twitch-based GFP−RFP FRET GECIs, which emerged during the development of Twitch−NR but were not further improved because their high K_d values made them unsuitable for neuronal imaging.[11] The larger K_d values of Twitch−NR and Twitch−GmRR can be explained by their larger k_{off} than Twitch 2B (Figure S5). Twitch−NR and Twitch−GmRR at 20 μM showed elution volumes corresponding to the molecular weight estimated from the amino acid sequences by size exclusion chromatography, supporting the monomeric state, at least up to this concentration range (Figure S6).

To evaluate the fluorescence intensities in mammalian cells for FRET ratio imaging, we compared the intensities of Twitch−GmRR and Twitch−NR, whose K_d is an intermediate between that of Twitch−2B for cytosolic imaging and our Twitch−GmRR, in HeLa cells. Cells were coexpressed Twitch and reference miRFP using P2A peptide linker, and the intensities of the Twitch variants normalized to those of miRFP were compared for both the donor and acceptor detection channels under donor excitation. For both the donor and acceptor channels, Twitch−GmRR showed a significantly higher intensity than that of Twitch−NR (Figure 2B). The averaged intensities of Twitch−GmRR for the donor and acceptor channels were 2.2- and 4.2-times greater than those of Twitch−NR, respectively, and the greater difference in the red channel is thought to be due to the higher FRET efficiency of Twitch−GmRR. In addition to the intensity, we evaluated the photostability of the Twitch variants. The photobleaching time constants of Twitch−GmRR (donor: 9149 s; acceptor: 1672 s) under donor excitation were longer than those of Twitch−NR (donor: 1560 s; acceptor: 1012 s) for both donor and acceptor channels (Figure S7). The large difference in donor photostability (approximately 5.9-times) reflects the higher photostability of Gamillus than that of circularly permuted mNeonGreen. Considering the less photostability of Gamillus than normal mNeonGreen reported by direct comparison,[19] this would be due to the effect of introducing circular permutation into mNeonGreen, suggesting the advantage of using noncircularly permuted FPs. Notably, the large difference between the donor and acceptor photostabilities in Twitch−GmRR can cause a time-dependent decrease in the intensity ratio owing to the faster photobleaching of the RRvT for imaging in a photobleaching-dominant environment.

Time-Lapse Ca^{2+} Imaging of Live Cells with Twitch−GmRR. To evaluate the in-cell response of Twitch−GmRR, we performed imaging of histamine-induced Ca^{2+} concentration changes in living HeLa cells, which is conventionally used as a proof-of-concept experiment to evaluate GECIs in the cytosol.[20] After stimulation using the histamine solution, the fluorescence intensity ratio in HeLa cells expressing Twitch−GmRR was immediately increased, and a subsequent oscillation of a smaller ratio was observed, similar to that of GECIs for the cytosol (Figure 3A and B; Figure S8). Although the K_d (1.41 μM) is slightly higher than the estimated concentration range of histamine-induced Ca^{2+} changes in HeLa cells (100 nM to 1 μM),[21] Twitch−GmRR showed an increase in the ratio. The ratio difference of the first peak from the baseline ($R_{max} - R_0$) averaged approximately 80% of that of the baseline (R_0). Subsequent Ca^{2+} oscillations were also detected as independent peaks, indicating that Twitch−GmRR has a temporal resolution comparable to that of previously

https://doi.org/10.1021/acssensors.3c02398
ACS Sens. 2024, 9, 1743−1748

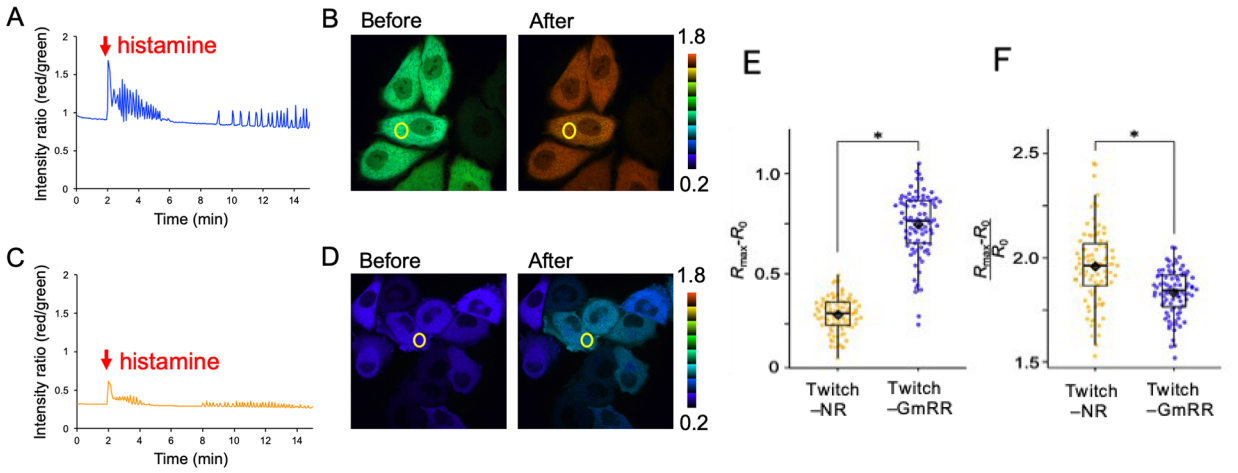

Figure 3. Ca^{2+} imaging of the histamine response in HeLa cells expressing Twitch−GmRR and Twitch−NR. Representative time-lapse imaging results of HeLa cells expressing Twitch−GmRR (A, B) or Twitch−NR (C, D). (A, C) Time course of the fluorescence ratio (green/red) in the area enclosed by the yellow ellipsoids on the cell in images B or D. Timing of histamine solution addition is indicated by red arrows. (B, D) Fluorescence ratio images immediately before (left) and after (right) the addition of histamine solution. Images were displayed by IMD (Intensity Modulated Display mode) in 8 ratios with 32 intensities. Scale bar: 20 μm. (E, F) Dot plot overlaid a box plot of the ratio difference of the first peak from baseline ($R_{max} - R_0$) (E), and the dynamic range $\frac{R_{max} - R_0}{R_0}$ (F) of Twitch−NR and Twitch−GmRR. Black diamonds indicate the mean values (*$p < 0.05$, two-sided Wilcoxon rank-sum test; $n = 87$ cells for each). Results for 87 cells from 12 dish cultures are shown for both Twitch−NR and Twitch−GmRR.

developed GECIs for cytosolic Ca^{2+} imaging. Compared to Twitch−NR, which could also detect the histamine response (Figure 3C and D; Figure S8), the average $R_{max} - R_0$ value of Twitch−GmRR was 2.5-times higher (Figure 3E). In principle, when K_d was largely shifted away from the range of Ca^{2+} changes in the target phenomena, the ratio change became smaller. Therefore, the larger $R_{max} - R_0$ of Twitch−GmRR, despite its larger K_d shift than that of Twitch−NR, must be attributed to the larger dynamic range of Twitch−GmRR. Meanwhile, the dynamic range $\frac{R_{max} - R_0}{R_0}$ for the first peak of Twitch−GmRR was 0.94-times that of Twitch−NR (Figure 3F), which was caused by the higher baseline ratio of Twitch−GmRR (Figure 3A and C). Further experiments are needed to more accurately assess the dynamic range in the cells. Here, we intentionally selected an inappropriate Ca^{2+} range for Twitch−GmRR to evaluate its versatility for cytosolic imaging. However, when imaging for the appropriate Ca^{2+} range, such as mitochondrial Ca^{2+} dynamics, which was imaged by GECIs with μM K_d,[22] a much higher ratio change can be expected. Further modifications, mainly in the sensing domain, are required to generate affinity variants of Twitch−GmRR for efficient Ca^{2+} sensing in different Ca^{2+} ranges.

CONCLUSION

In this study, we developed a GECI with a new green−red FRET pair using GFP Gamillus with a unique trans-configuration chromophore as the FRET donor. We expected an improvement in the dynamic range greater than that of Twitch−NR, the current best performing green−red FRET. We combined Gamillus-based Twitch with RRvT. The Twitch−GmRR indicator had 1.5-times the dynamic range of Twitch−NR. Compared to the effort to develop Twitch−NR, which includes the selection of circularly permuted fluorescent proteins and linkers using an excellent screening system, the development of Twitch−GmRR was easier and it surpassed the dynamic range of other GFP−RFP FRET GECIs with fewer candidate noncircularly permuted FPs and linker combinations without iteratively looping the screening. Looking back at the exploration of GFP−RFP pairs with high FRET efficiency, RFPs with trans-configured chromophores (mRuby2 and mRuby3) have contributed to the generation of higher FRET pairs with GFP with a cis-configured chromophore.[8−10] Similarly, the trans chromophore in Gamillus may improve the dynamic range by modulating the FRET efficiency by changing the relative orientation of the chromophores due to changes in the cis−trans configuration. Therefore, the choice of the cis−trans isomer of the chromophore is important for the improvement of FRET indicators consisting of FPs, as is the selection of circular permutants and linker length. Although circular permutants of Gamillus with imaging quality are not currently available, once they are developed, the search space for improvement will expand, with a possibility to overcome this obstacle, which cannot be overcome by GFPs with cis-configuration chromophores.

Here, Twitch−GmRR showed superiority in sensing the dynamic range *in vitro*; however, its FP components have some drawbacks. Gamillus has a reversible photoswitching property that causes fluorescence to switch off under strong excitation light irradiation. Therefore, suppression of excitation light intensity or simultaneous irradiation of light within the wavelength range for switching on is required to prevent fluorescence attenuation.[13] RRvT is a tandem dimer fluorescent protein.[15] As the larger molecular size of the red FP moiety may cause problems such as fusion with other proteins or signal peptide sequences, the molecular design should be well considered. In addition, tdTomato, an ancestral FP of RRvT, exhibits slow maturation, resulting in cell diversity of maturation stages in transient expression, thereby affecting the FRET efficiency.[23] RRvT also requires a sufficient maturation time before the quantitative imaging of transiently expressed cells. Therefore, further improvement of Gamillus and RRvT can facilitate stable and user-friendly imaging by

https://doi.org/10.1021/acssensors.3c02398
ACS Sens. 2024, 9, 1743−1748

improving Twitch−GmRR or the newly developed Gamilus-RRvT FRET-based indicators in the future.

■ ASSOCIATED CONTENT

Supporting Information

The Supporting Information is available free of charge at https://pubs.acs.org/doi/10.1021/acssensors.3c02398.

Methods, selection of the FRET acceptor, dynamic range of Gamillus−tdTomato FRET GECIs, comparison of off-kinetics, analytical size exclusion chromatography, photobleaching measurements, histamine response in live cells, SDS-PAGE gel image of purified proteins, and amino acid sequence of Twitch-GmRR (PDF)

■ AUTHOR INFORMATION

Corresponding Authors

Tomoki Matsuda − *SANKEN, Osaka University, Ibaraki, Osaka 567-0047, Japan;* Present Address: Department of Biosciences, School of Science, Kitasato University, Sagamihara, Kanagawa 252-0373, Japan (after April 2024); Email: tmatsuda@sanken.osaka-u.ac.jp

Takeharu Nagai − *SANKEN, Osaka University, Ibaraki, Osaka 567-0047, Japan;* orcid.org/0000-0003-2650-9895; Email: ng1@sanken.osaka-u.ac.jp

Authors

Shinya Sakai − *SANKEN, Osaka University, Ibaraki, Osaka 567-0047, Japan*

Kei-ichi Okazaki − *Research Center for Computational Science, Institute for Molecular Science, National Institutes of Natural Sciences, Okazaki 444-8585, Japan; Graduate Institute for Advanced Studies, SOKENDAI, Okazaki, Aichi 444-8585, Japan;* orcid.org/0000-0003-2168-3069

Complete contact information is available at: https://pubs.acs.org/10.1021/acssensors.3c02398

Author Contributions

T.M., S.S., and T.N. were involved in the initial design of the indicators. K.O. suggested using linker sequences from a structural perspective. S.S. and T.M. established the DNA constructs and evaluated the FRET efficiency and dynamic range *in vitro*. T.M. performed *in vitro* Ca^{2+} titration and live cell imaging and analyzed the data. T.M. prepared the figures and drafted the manuscript. All the authors contributed to the editing and proofreading of the manuscript. T.M. and T.N. reviewed all aspects of the project. All authors approved the final version of the manuscript.

Funding

This work was supported by MEXT Grant-in-Aid for Transformative Research Areas (A) "Integration of extracellular information by multimodal ECM activity" (No. 23H04935) to T.M., Scientific Research on Innovative Areas "Singularity biology" (No. 18H05410) to T.N., JST CREST Program (No. JPMJCR20E4) to T.M., and the grant of Joint Research by the National Institutes of Natural Sciences (NINS; No. 01112105) to T.N. and K.O. K.O. was supported by Building of Consortia for the Development of Human Resources in Science and Technology, MEXT, Japan.

Notes

The authors declare no competing financial interest.

■ REFERENCES

(1) Carlson, H. J.; Campbell, R. E. Genetically Encoded FRET-Based Biosensors for Multiparameter Fluorescence Imaging. *Curr. Opin. Biotechnol.* **2009**, *20* (1), 19−27.

(2) Nagai, T.; Yamada, S.; Tominaga, T.; Ichikawa, M.; Miyawaki, A. Expanded Dynamic Range of Fluorescent Indicators for Ca(2+) by Circularly Permuted Yellow Fluorescent Proteins. *Proc. Natl. Acad. Sci. U. S. A.* **2004**, *101* (29), 10554−10559.

(3) Horikawa, K.; Yamada, Y.; Matsuda, T.; Kobayashi, K.; Hashimoto, M.; Matsu-ura, T.; Miyawaki, A.; Michikawa, T.; Mikoshiba, K.; Nagai, T. Spontaneous Network Activity Visualized by Ultrasensitive Ca(2+) Indicators, Yellow Cameleon-Nano. *Nat. Methods.* **2010**, *7* (9), 729−732.

(4) Thestrup, T.; Litzlbauer, J.; Bartholomäus, I.; Mues, M.; Russo, L.; Dana, H.; Kovalchuk, Y.; Liang, Y.; Kalamakis, G.; Laukat, Y.; Becker, S.; Witte, G.; Geiger, A.; Allen, T.; Rome, L. C.; Chen, T. W.; Kim, D. S.; Garaschuk, O.; Griesinger, C.; Griesbeck, O. Optimized Ratiometric Calcium Sensors For Functional *In Vivo* Imaging of Neurons and T Lymphocytes. *Nat. Methods.* **2014**, *11* (2), 175−182.

(5) Wäldchen, S.; Lehmann, J.; Klein, T.; van de Linde, S.; Sauer, M. Light-Induced Cell Damage in Live-Cell Super-Resolution Microscopy. *Sci. Rep.* **2015**, *5*, 15348.

(6) Yang, C.; Hou, V. W.; Girard, E. J.; Nelson, L. Y.; Seibel, E. J. Target-to-Background Enhancement in Multispectral Endoscopy with Background Autofluorescence Mitigation for Quantitative Molecular Imaging. *J. Biomed. Opt.* **2014**, *19* (7), 076014.

(7) Lifante, J.; Shen, Y.; Ximendes, E.; Rodríguez, E. M.; Ortgies, D. H. The Role of Tissue Fluorescence in In Vivo Optical Bioimaging. *J. Appl. Phys.* **2020**, *128*, 171101.

(8) Lam, A. J.; St-Pierre, F.; Gong, Y.; Marshall, J. D.; Cranfill, P. J.; Baird, M. A.; McKeown, M. R.; Wiedenmann, J.; Davidson, M. W.; Schnitzer, M. J.; Tsien, R. Y.; Lin, M. Z. Improving FRET Dynamic Range with Bright Green and Red Fluorescent Proteins. *Nat. Methods.* **2012**, *9* (10), 1005−1012.

(9) Bajar, B. T.; Wang, E. S.; Lam, A. J.; Kim, B. B.; Jacobs, C. L.; Howe, E. S.; Davidson, M. W.; Lin, M. Z.; Chu, J. Improving Brightness and Photostability of Green and Red Fluorescent Proteins for Live Cell Imaging and FRET Reporting. *Sci. Rep.* **2016**, *6*, 20889.

(10) Shen, Y.; Wu, S. Y.; Rancic, V.; Aggarwal, A.; Qian, Y.; Miyashita, S. I.; Ballanyi, K.; Campbell, R. E.; Dong, M. Genetically Encoded Fluorescent Indicators for Imaging Intracellular Potassium Ion Concentration. *Commun. Biol.* **2019**, *2*, 18.

(11) Zhang, D.; Redington, E.; Gong, Y. Rational Engineering of Ratiometric Calcium Sensors with Bright Green and Red Fluorescent proteins. *Commun. Biol.* **2021**, *4* (1), 924.

(12) Gohil, K.; Wu, S.-Y.; Takahashi-Yamashiro, K.; Shen, Y.; Campbell, R. E. Biosensor Optimization Using a Förster Resonance Energy Transfer Pair Based on mScarlet Red Fluorescent Protein and an mScarlet-Derived Green Fluorescent Protein. *ACS Sens.* **2023**, *8* (2), 587−597.

(13) Shinoda, H.; Ma, Y.; Nakashima, R.; Sakurai, K.; Matsuda, T.; Nagai, T. Acid-Tolerant Monomeric GFP from Olindias formosa. *Cell Chem. Biol.* **2018**, *25* (3), 330−338.e7.

(14) Trigo-Mourino, P.; Thestrup, T.; Griesbeck, O.; Griesinger, C.; Becker, S. Dynamic Tuning of FRET in a Green Fluorescent Protein Biosensor. *Sci. Adv.* **2019**, *5* (8), eaaw4988.

(15) Wiens, M. D.; Shen, Y.; Li, X.; Salem, M. A.; Smisdom, N.; Zhang, W.; Brown, A.; Campbell, R. E. A Tandem Green-Red Heterodimeric Fluorescent Protein with High FRET Efficiency. *Chembiochem.* **2016**, *17* (24), 2361−2367.

(16) Lakowicz, J. R. *Principles of Fluorescence Spectroscopy*, 3rd ed.; Springer: New York, 2006; pp 443−449.

(17) Carlson, H. J.; Campbell, R. E. Genetically Encoded FRET-Based Biosensors for Multiparameter Fluorescence Imaging. *Curr. Opin. Biotechnol.* **2009**, *20* (1), 19−27.

(18) Watabe, T.; Terai, K.; Sumiyama, K.; Matsuda, M. Booster, a Red-Shifted Genetically Encoded Förster Resonance Energy Transfer (FRET) Biosensor Compatible with Cyan Fluorescent Protein/

Yellow Fluorescent Protein-Based FRET Biosensors and Blue Light-Responsive Optogenetic Tools. *ACS Sens.* **2020**, *5* (3), 719−730.
(19) Petrich, A.; Aji, A. K.; Dunsing, V.; Chiantia, S. Benchmarking of novel green fluorescent proteins for the quantification of protein oligomerization in living cells. *PLoS One* **2023**, *18* (8), No. e0285486.
(20) Zhao, Y.; Araki, S.; Wu, J.; Teramoto, T.; Chang, Y. F.; Nakano, M.; Abdelfattah, A. S.; Fujiwara, M.; Ishihara, T.; Nagai, T.; Campbell, R. E. An Expanded Palette of Genetically Encoded Ca^{2+} Indicators. *Science* **2011**, *333* (6051), 1888−1891.
(21) Maeshima, K.; Matsuda, T.; Shindo, Y.; Imamura, H.; Tamura, S.; Imai, R.; Kawakami, S.; Nagashima, R.; Soga, T.; Noji, H.; Oka, K.; Nagai, T. A Transient Rise in Free Mg^{2+} Ions Released from ATP-Mg Hydrolysis Contributes to Mitotic Chromosome Condensation. *Curr. Biol.* **2018**, *28* (3), 444−451.
(22) Suzuki, J.; Kanemaru, K.; Iino, M. Genetically Encoded Fluorescent Indicators for Organellar Calcium Imaging. *Biophys. J.* **2016**, *111* (6), 1119−1131.
(23) van der Krogt, G. N.; Ogink, J.; Ponsioen, B.; Jalink, K. A Comparison of Donor-Acceptor Pairs for Genetically Encoded FRET Sensors: Application to the Epac cAMP Sensor as an Example. *PLoS One.* **2008**, *3* (4), e1916.

https://doi.org/10.1021/acssensors.3c02398
ACS Sens. 2024, 9, 1743−1748